



## Article

# Fluorescence Properties of ZnOQDs-GO-g-C<sub>3</sub>N<sub>4</sub> Nanocomposites

Tianze Liu <sup>1,†</sup> , Lei Wang <sup>2,†</sup>, Ruxue Jiang <sup>2</sup>, Yashi Tang <sup>2</sup>, Yuxin He <sup>2</sup>, Changze Sun <sup>3</sup>, Yuguang Lv <sup>2,\*</sup> and Shuang Liu <sup>4,\*</sup>

<sup>1</sup> College of Clinical Medicine, Jiamusi University, Jiamusi 154007, China

<sup>2</sup> College of Pharmacy, Jiamusi University, Jiamusi 154007, China

<sup>3</sup> School of Mechanical Engineering, Jiamusi University, Jiamusi 154007, China

<sup>4</sup> College of Basic Medicine, Jiamusi University, Jiamusi 154007, China

\* Correspondence: yuguanglv@163.com (Y.L.); lius@jmsu.edu.cn (S.L.)

† These authors contributed equally to this work.

**Abstract:** In this paper, the fluorescence properties of ZnOQD-GO-g-C<sub>3</sub>N<sub>4</sub> composite materials (ZCGQDs) were studied. Firstly, the addition of a silane coupling agent (APTES) in the synthesis process was explored, and it was found that the addition of 0.04 g·mL<sup>-1</sup> APTES had the largest relative fluorescence intensity and the highest quenching efficiency. The selectivity of ZCGQDs for metal ions was also investigated, and it was found that ZCGQDs showed good selectivity for Cu<sup>2+</sup>. ZCGQDs were optimally mixed with Cu<sup>2+</sup> for 15 min. ZCGQDs also had good anti-interference capability toward Cu<sup>2+</sup>. There was a linear relationship between the concentration of Cu<sup>2+</sup> and the fluorescence intensity of ZCGQDs in the range of 1~100 μM. The regression equation was found to be  $F_0/F = 0.9687 + 0.12343C$ . The detection limit of Cu<sup>2+</sup> was about 1.74 μM. The quenching mechanism was also analyzed.

**Keywords:** nanocomposites; fluorescence probe; metal ion; fluorescence properties



**Citation:** Liu, T.; Wang, L.; Jiang, R.; Tang, Y.; He, Y.; Sun, C.; Lv, Y.; Liu, S. Fluorescence Properties of ZnOQDs-GO-g-C<sub>3</sub>N<sub>4</sub> Nanocomposites. *Micromachines* **2023**, *14*, 711. <https://doi.org/10.3390/mi14040711>

Academic Editor: Songkil Kim

Received: 4 March 2023

Revised: 17 March 2023

Accepted: 20 March 2023

Published: 23 March 2023



**Copyright:** © 2023 by the authors. Licensee MDPI, Basel, Switzerland. This article is an open access article distributed under the terms and conditions of the Creative Commons Attribution (CC BY) license (<https://creativecommons.org/licenses/by/4.0/>).

## 1. Introduction

ZnO is an eco-friendly oxide semiconductor, and compared with traditional CdSe or CdTe quantum dots, it is an inexpensive luminescent material, which makes it more attractive in practical applications [1–3]. Over the past few years, a variety of physical and chemical synthesis techniques have been developed to synthesize ZnO QDS. Various chemical methods have been developed to synthesize ZnO nanocrystals, and many research groups have used the sol–gel method to improve the process of obtaining ZnO quantum dots with different sizes and fluorescence characteristics [4]. ZnO quantum dots have been widely used in the photoelectric field [5–7], biomedical field [8] energy electrochemical field [9–12], fluorescence imaging [13], gas sensing [14] selective detection [15], and other fields.

Graphene oxide (GO) is a carbon-based nanomaterial widely used for adsorption and catalytic degradation due to its high specific surface area and tunable structure [16]. It is also a promising nanomaterial for a wide range of applications, including but not limited to energy storage [17,18], electrical sensors [19,20], and antimicrobial activity [21,22]. GO exhibits excellent performance in photocatalytic activity due to its high electron mobility, good electrical conductivity and chemical stability. GO can be involved in the synthesis of various composite materials, such as nanoparticles, polymers, and novel metal–organic frame-derived materials, which can be used in separation [23], catalysis [24], electrochemical devices [25], and coatings [26].

In recent decades, a type of non-metallic semiconductor graphitic carbon nitride (g-C<sub>3</sub>N<sub>4</sub>) has attracted great attention among researchers worldwide because it has good photocatalytic activity under visible light irradiation and shows great potential in various environmental remediation applications. As a visible light-responsive non-metallic

organic semiconductor, it has been widely used in sewage treatment [27], CO<sub>2</sub> reduction [28,29], hydrogen production from water photolysis [30,31] energy conversion [32,33], and other fields.

Yang [34] et al. established a highly efficient and stable Al<sup>3+</sup> fluorescent probe using the fluorescent “on” mode of zinc sulfide crystal composite zinc oxide quantum dots (ZnS/ZnOQDs). The as-synthesized ZnS/ZnOQDs exhibited fluorescence enhancement for Al, confirming the availability of fluorescence sensing probes.

Copper is a toxic heavy metal element. Cu<sup>2+</sup> is involved in many reaction activities in the human body and plays an important role in various physiological processes such as the formation of red blood cells and the normal growth and maintenance of brain tissue, kidney, heart, and other organs of the body [35]. However, the content of Cu<sup>2+</sup> is also a double-edged sword, and the excess or deficiency of Cu<sup>2+</sup> can lead to the disorder of cellular homeostasis and damage the central nervous system. The abnormal accumulation of Cu<sup>2+</sup> will lead to the appearance of some human diseases, including Alzheimer’s disease, Parkinson’s disease, Menkes disease, and Wilson’s disease. If Cu<sup>2+</sup> is deficient in the human body, gastrointestinal diseases and abnormal bone growth will occur [36].

Copper accumulation in the body will produce certain harm [37]. In addition, heavy metal ions affect the activities of proteins and enzymes in the human body and accumulate in some organs, resulting in chronic poisoning [38]. Heavy metal pollution seriously endangers human health, which has raised great concern in the world. Therefore, it is of great significance and urgency to develop a rapid and sensitive detection method for heavy metal ions for environmental and public safety.

The traditional detection methods of heavy metal ions include electrochemical analysis [39,40], atomic absorption spectroscopy [41], atomic emission spectroscopy, inductively coupled plasma mass spectrometry [42], and surface-enhanced Raman spectroscopy [43,44], but these methods have the problems of cumbersome detection steps, high instrument costs, difficulty in real-time detection, and low sensitivity. Their application in the field of heavy metal ion detection is greatly restricted [45]. Compared with traditional detection methods, fluorescence analysis methods have the advantages of high resolution, good sensitivity and rapid response, and have strong potential for application. In most cases, the fluorescence intensity of fluorescent probes is related to metal ions, so it is relatively easy to qualitatively and quantitatively analyze heavy metal ions by measuring the fluorescence intensity [46]. Therefore, it is of great significance to develop fluorescent probes that can selectively detect important metal ions such as copper.

In this paper, the selectivity of ZnOQD-GO-g-C<sub>3</sub>N<sub>4</sub> composite materials (ZCGQDs) for metal ions and the mixing time, anti-interference ability, linear relationship, and fluorescence quenching mechanism of ZCGQDs composite materials and the target metal ion Cu<sup>2+</sup> were analyzed, which provides a new idea for the research of zinc oxide quantum dots.

## 2. Experimental

### 2.1. Experimental Reagents

The inorganic compounds containing Al<sup>3+</sup>, Ba<sup>2+</sup>, Ca<sup>2+</sup>, Cd<sup>2+</sup>, Co<sup>2+</sup>, Cr<sup>3+</sup>, Cu<sup>2+</sup>, Fe<sup>2+</sup>, Fe<sup>3+</sup>, Hg<sup>2+</sup>, Mn<sup>2+</sup>, Mg<sup>2+</sup>, Ni<sup>2+</sup>, Pb<sup>2+</sup>. AlCl<sub>3</sub>, BaCl<sub>2</sub>, CaCl<sub>2</sub>, CdCl<sub>2</sub>·25H<sub>2</sub>O, CoCl<sub>2</sub>·6H<sub>2</sub>O, CuCl<sub>2</sub>·2H<sub>2</sub>O, CrCl<sub>3</sub>·6H<sub>2</sub>O, FeCl<sub>2</sub>·4H<sub>2</sub>O, Fe(NO<sub>3</sub>)<sub>3</sub>·9H<sub>2</sub>O, HgCl<sub>2</sub>, Mn(NO<sub>3</sub>)<sub>2</sub>·4H<sub>2</sub>O, Mg(NO<sub>3</sub>)<sub>2</sub>·6H<sub>2</sub>O, NiCl<sub>2</sub>·6H<sub>2</sub>O, and Pb(NO<sub>3</sub>)<sub>2</sub> were purchased from Sinopharm Chemical Reagent Co., Ltd. (Huai’an, China).

### 2.2. Metal Ion Detection

#### 2.2.1. Selective Detection of Metal Ions Based on ZCGQDs

- a. The inorganic compounds containing Al<sup>3+</sup>, Ba<sup>2+</sup>, Ca<sup>2+</sup>, Cd<sup>2+</sup>, Co<sup>2+</sup>, Cr<sup>3+</sup>, Cu<sup>2+</sup>, Fe<sup>2+</sup>, Fe<sup>3+</sup>, Hg<sup>2+</sup>, Mn<sup>2+</sup>, Mg<sup>2+</sup>, Ni<sup>2+</sup>, and Pb<sup>2+</sup> were used as metal ion sources, dissolved in deionized water to prepare 50 mM solutions of different metal ions;

- b. A pipette was used to accurately pipette 0.005 mL of different metal ion solutions of the same concentration configured in step a;
- c. Then, 4.995 mL of the prepared ZCGQDs composite sample was taken;
- d. Various metal ions were added to the ZCGQDs composite sample to obtain a 50  $\mu\text{M}$  colloidal solution of different metal ions and left for 20 min;
- e. A quartz cuvette was used, with a diameter of 1 cm and transparent on all sides, and the different metal ion colloid solutions in step d were added;
- f. The mixed colloidal solutions were scanned to obtain their fluorescence spectra and intensity values. To reduce systematic errors, each mixed colloidal solution was scanned three times, and the average was calculated as the final intensity result.

The fluorescence intensities of different mixed colloidal solutions were compared to determine the selectivity of the fluorescent probes for metal ions.

### 2.2.2. Determination of the Linear Relationship between ZCGQDs and Target Metal Ion $\text{Cu}^{2+}$

In order to explore the selectivity of the prepared ZCGQDs complexes to  $\text{Cu}^{2+}$ , the relationship between  $\text{Cu}^{2+}$  concentration and the change in the fluorescence intensity of the ZCGQDs complexes was investigated.

Experimental process:

- a.  $\text{Cu}^{2+}$  was derived from the  $\text{CuCl}_2 \cdot 2\text{H}_2\text{O}$  inorganic compound, which was dissolved in deionized water, and several solutions with different concentrations of  $\text{Cu}^{2+}$  were prepared using the stepwise dilution method;
- b. A pipette was used to accurately pipette 0.005 mL of  $\text{Cu}^{2+}$  solutions at the different concentrations configured in step a;
- c. Then, 4.995 mL samples of the ZCGQDs composites were taken;
- d. Different concentrations of  $\text{Cu}^{2+}$  solution were added to the ZCGQDs composite sample, mixed and shaken well to obtain a colloidal solution, which was left for 15 min;
- e. A quartz cuvette was used, with a diameter of 1 cm and transparent on all sides, and the colloidal solutions with different concentrations of  $\text{Cu}^{2+}$  in step d were added;
- f. The mixed colloidal solutions were scanned to obtain their fluorescence spectra and intensity values. In order to reduce systematic errors, each mixed colloidal solution was scanned three times, and the average intensity value was used as the representative.

### 2.3. Experimental Optimization

The addition of metal ions can cause the fluorescence intensity of ZCGQDs complexes to weaken, resulting in a fluorescence quenching phenomenon. Among these metal ions, the fluorescence intensity of the solution changed most significantly after the addition of  $\text{Cu}^{2+}$ . Using this principle, the ZCGQDs complexes were used as fluorescent probes to detect  $\text{Cu}^{2+}$ . However, it should be noted that there were differences in experimental settings, and different quenching efficiencies were obtained. We optimized the experiment in two aspects: (a) the addition of different concentrations of APTES in the preparation of ZCGQDs complexes; (b) the mixing of ZCGQDs complexes and  $\text{Cu}^{2+}$  at different times.

## 3. Results and Discussion

### 3.1. Effect of APTES Concentration Used to Synthesize ZCGQDs

In order to explore the effect of the addition of different concentrations of APTES on the quenching efficiency during the preparation of synthetic ZCGQDs complexes, the experiments were conducted as follows: (a) During the preparation of the ZCGQDs composites, 0.02  $\text{g} \cdot \text{mL}^{-1}$ , 0.04  $\text{g} \cdot \text{mL}^{-1}$ , 0.06  $\text{g} \cdot \text{mL}^{-1}$ , and 0.08  $\text{g} \cdot \text{mL}^{-1}$  of a silane coupling agent (APTES) were added; (b) the ZCGQDs complexes were scanned with a fluorescence spectrophotometer to obtain their fluorescence spectra and fluorescence peak intensity values; (c) The fluorescence intensity changes of the solutions before and after the addition

of  $\text{Cu}^{2+}$  were measured, and the fluorescence intensity values were labeled as  $F_0$  and  $F$ , respectively; the corresponding fluorescence quenching rates were represented by  $F_0/F$ . To reduce systematic errors, the above procedure was repeated three times and the average fluorescence intensity values were calculated.

From Figure 1a, it can be concluded that with the increase in the APTES concentration, the fluorescence intensity of the ZCGQDs complexes increased. However, when the APTES concentration increased to a certain extent, the fluorescence intensity decreased instead of increasing. The reason may be that the luminescence of ZnOQDs in the visible light range is due to the deep-level emission caused by lattice defects. This is mainly caused by two kinds of defects: (1) Starting from the lower part of the conduction band, the electrons gradually leap toward the  $\text{O}_{\text{Zn}}$  and  $\text{O}_{\text{i}}$  deep body defects; (2) starting from the deep body defect  $\text{V}_{\text{O}}$ , the electrons gradually leap to the upper end of the valence band. Therefore, there should be a certain concentration range and an optimum value. As shown in Figure 1a, which illustrates the change in the APTES concentration and the fluorescence intensity of the ZCGQDs complexes, the wavelength blue shift occurred when the APTES concentration exceeded  $0.02 \text{ g}\cdot\text{mL}^{-1}$ , which indicates that the appropriate increase in the APTES concentration was beneficial to the ZCGQDs complexes. The surface quickly formed a coating, which in turn reduced the agglomeration of the ZCGQDs complexes. By adding  $0.04 \text{ g}\cdot\text{mL}^{-1}$  APTES, the fluorescence intensity was the highest.

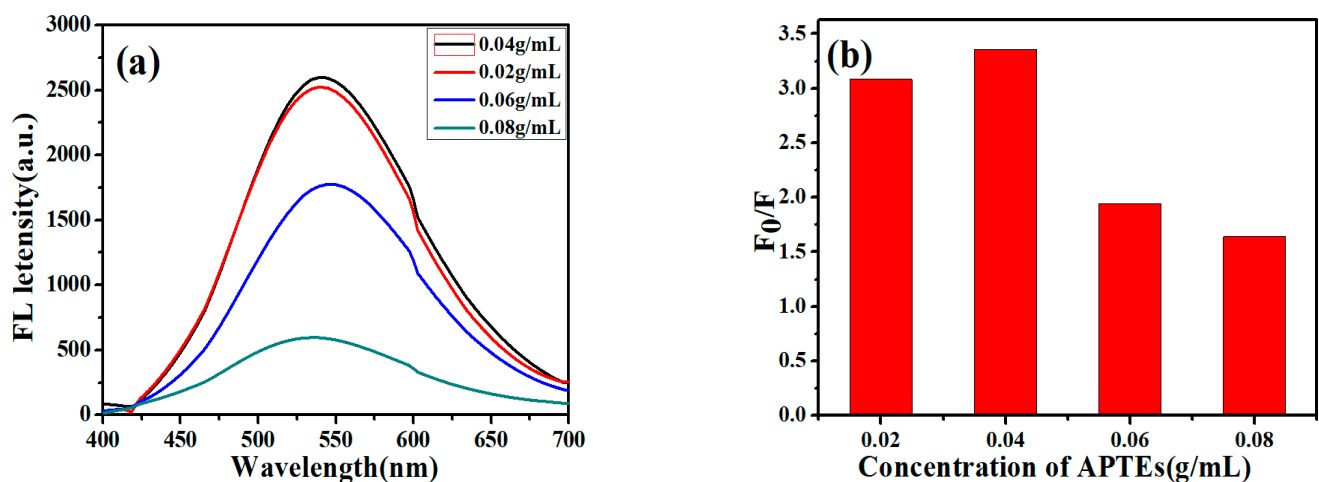


**Figure 1.** (a) Fluorescence emission spectra of ZCGQDs; (b) relative fluorescence intensity with the addition of  $20 \mu\text{M}$   $\text{Cu}^{2+}$  to ZCGQDs.

Figure 1b shows the relative fluorescence intensity values after the addition of equal amounts of  $\text{Cu}^{2+}$  ( $20 \mu\text{M}$ ) to the complexes formed by different concentrations of APTES and ZCGQDs. With the increase in the APTES concentration, the agglomeration degree of the ZCGQDs complexes weakened, the relative fluorescence intensity increased, and the quenching efficiency increased. However, when the APTES concentration increased to a certain extent, the relative fluorescence intensity did not increase but decreased. The excessive increase in the APTES concentration caused the coating layer of the ZCGQDs complexes to be too thick, thus destroying the fluorescence emission of the quantum dots caused by surface defects, decreasing the relative fluorescence intensity, and reducing the quenching efficiency. Notably,  $0.04 \text{ g}\cdot\text{mL}^{-1}$  APTES had the highest relative fluorescence intensity and the highest quenching efficiency. Therefore, the concentration of  $0.04 \text{ g}\cdot\text{mL}^{-1}$  APTES was selected to synthesize the ZCGQDs complexes for subsequent experimental analysis.

### 3.2. Effect of Mixing Time of ZCGQDs and $\text{Cu}^{2+}$

As shown in Figure 2, nine time points were selected from 5 to 45 min to determine the extent of the fluorescence quenching of  $\text{Cu}^{2+}$  and ZCGQDs complexes at different mixing times [47,48]. In the range of 5–15 min, the quenching efficiency enhanced with increasing

time and remained basically stable after 15 min. The highest efficiency was reached at 15 min. In order to improve the fluorescence properties of the ZCGQDs complexes in subsequent experiments, a fixed mixing time of 15 min was selected.

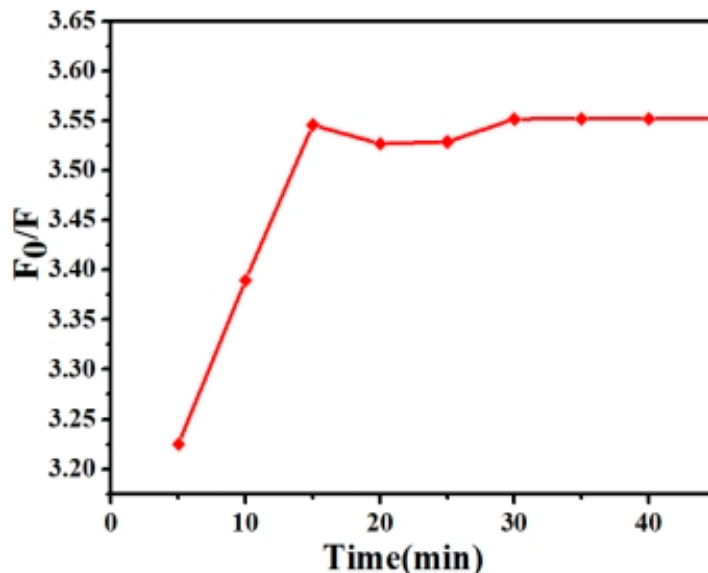


Figure 2. The plot of relative fluorescence intensity versus time.

### 3.3. Selectivity of ZCGQDs to Metal Ions

Equal concentrations of various metal ions were added to the ZCGQDs composite sample to obtain a 50 μM colloidal solution of different metal ions and allowed to stand for 15 min [49]. The changes in the fluorescence intensity of the ZCGQDs complexes before and after the addition of  $\text{Cu}^{2+}$  were measured. The fluorescence intensity values were marked as  $F_0$  and  $F$ , and the corresponding fluorescence quenching rate was expressed as  $F_0/F$ . In order to reduce the systematic error, the above process was repeated three times, and the fluorescence average intensity values were calculated.

Figure 3a,b show the effects of different metal ions on the fluorescence intensity of the ZCGQDs complexes under the same concentration conditions. It was found that  $\text{Cu}^{2+}$  resulted in a marked fluorescence quenching phenomenon on the ZCGQDs complexes, and the as-prepared ZCGQDs complexes exhibited good selectivity toward  $\text{Cu}^{2+}$ .

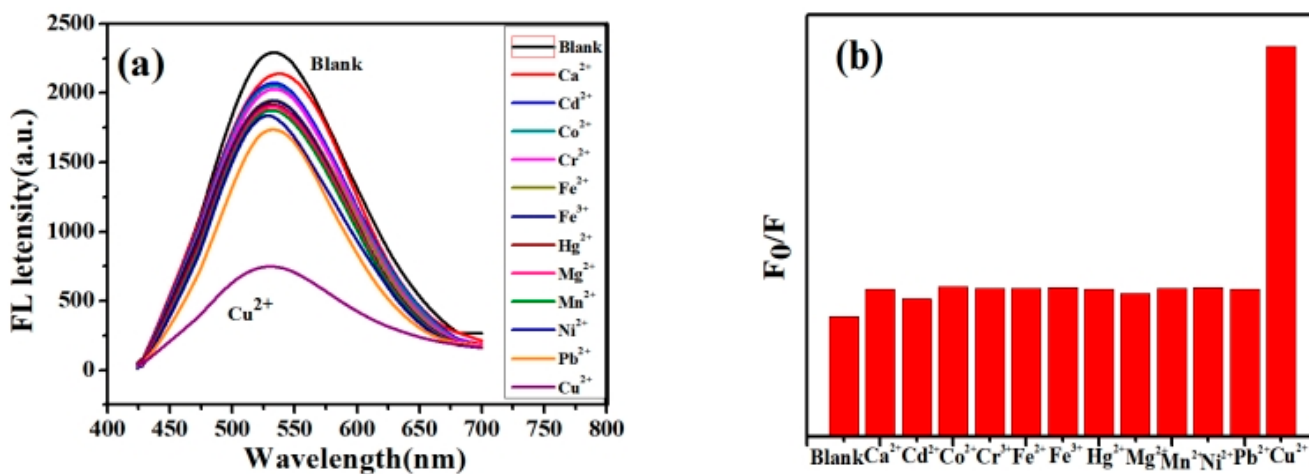
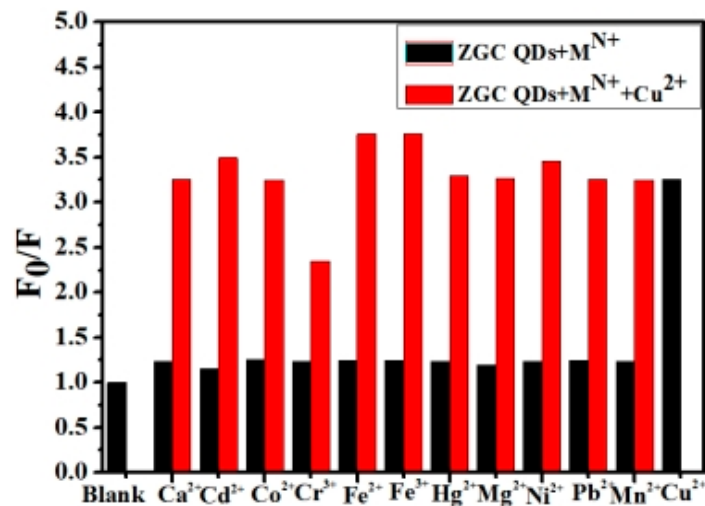


Figure 3. (a) Fluorescence spectra of the different heavy metal ions added; (b) relative fluorescence intensity of the different heavy metal ions added.

### 3.4. Anti-Interference Performance of ZCGQDs on $\text{Cu}^{2+}$

Different metal ions of equal concentration were prepared and added to ZCGQDs composite samples, and the mixtures were shaken to obtain the colloidal solutions of the different metal ions. Then,  $\text{Cu}^{2+}$  was added to the solutions and shaken well, and the mixtures were left to stand for 15 min to test their anti-interference performance [47]. The changes in the fluorescence intensity of the ZCGQDs complexes before and after the addition of  $\text{Cu}^{2+}$  were measured. The fluorescence intensity values were marked as  $F_0$  and  $F$ , and the relative fluorescence intensity (marked as  $F_0/F$ ) was used to represent the corresponding fluorescence quenching rate. In order to reduce the systematic error, the above process was repeated three times, and the average fluorescence intensity values were calculated. As shown in Figure 4,  $\text{Cu}^{2+}$  still exhibited strong fluorescence quenching under the same concentration of different metals, and the fluorescence quenching efficiency did not significantly change compared with  $\text{Cu}^{2+}$  without interference, which indicates that the prepared ZCGQDs composites had good anti-interference capability toward  $\text{Cu}^{2+}$ .



**Figure 4.** Relative fluorescence intensity of ZCGQDs in the coexistence of  $\text{Cu}^{2+}$  with other metal ions.

### 3.5. Linear Relationship between ZCGQDs and $\text{Cu}^{2+}$ Concentration

The stepwise dilution method was used to obtain the  $\text{Cu}^{2+}$  solutions of different concentrations, which were added to the ZCGQDs composite samples, mixed, and shaken to obtain the colloidal solutions of copper ions, and the solutions were allowed to stand for 10 min [48,49]. The changes in the fluorescence intensity of the ZCGQDs complexes before and after the addition of  $\text{Cu}^{2+}$  were measured. The fluorescence intensity values were marked as  $F_0$  and  $F$ , and the relative fluorescence intensity (marked as  $F_0/F$ ) was used to represent the corresponding fluorescence quenching rate.

From Figure 5a, it can be concluded that the fluorescence intensity of the ZCGQDs complexes decreased sequentially with the increase in  $\text{Cu}^{2+}$  concentration. This shows a linear relationship between the concentration of  $\text{Cu}^{2+}$  and the fluorescence intensity of ZCGQDs complexes. As seen in Figure 5b, the linear regression equation for the concentration of  $\text{Cu}^{2+}$  between 1 and 100  $\mu\text{M}$  is  $F_0/F = 0.9788 + 0.12283C$  ( $R^2 = 0.9951$ ), where  $C$  represents the concentration of  $\text{Cu}^{2+}$  in the solution and  $R^2$  represents the correlation constant. Using this equation, the limit of detection for  $\text{Cu}^{2+}$  was obtained, which was about 1.74  $\mu\text{M}$ .

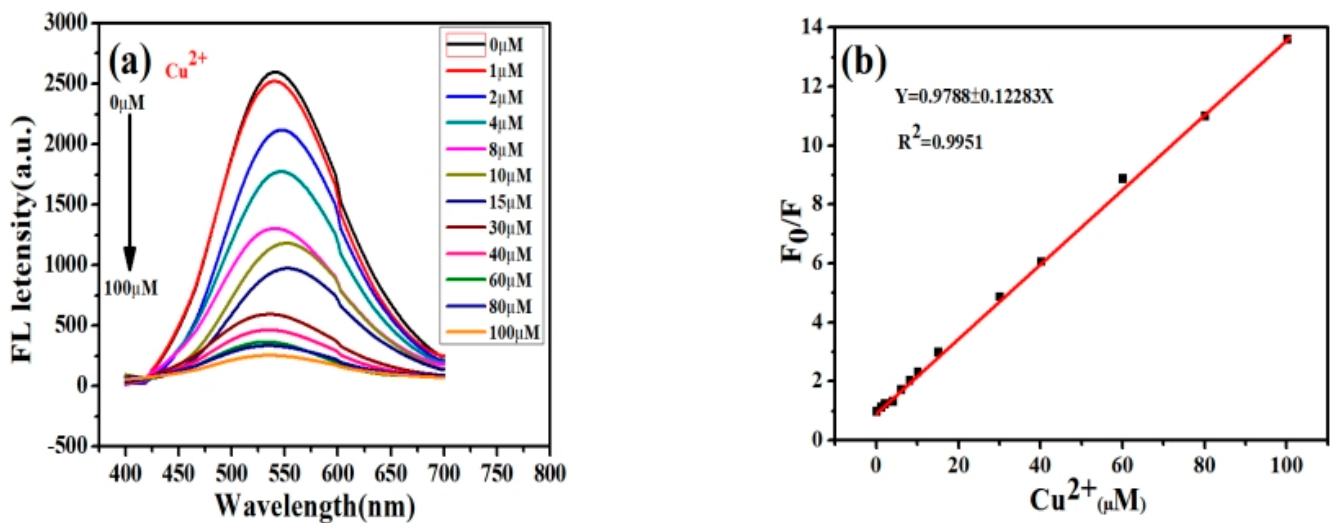


**Figure 5.** (a) Fluorescence spectra of different concentrations of  $\text{Cu}^{2+}$ ; (b) fitted curve of the linear relationship.

### 3.6. Analysis of Fluorescence Quenching Mechanism of ZCGQDs

Copper ions had a marked fluorescence quenching effect on the ZCGQDs complexes, and there was a strong linear relationship between the  $\text{Cu}^{2+}$  concentration and the relative fluorescence intensity of the ZCGQDs complexes.

Figure 6a,b shows the particle dispersion maps before and after the addition of  $\text{Cu}^{2+}$  to the ZCGQDs composite solution. A comparison was made using transmission electron microscopy and aggregation phenomenon was observed in the ZCGQDs composite, with a consequent weakening of the fluorescence intensity. Thus, the aggregation phenomenon in the ZCGQDs composite induced fluorescence quenching (AIQ) of the ZCGQDs complex, which was caused by  $\text{Cu}^{2+}$ .

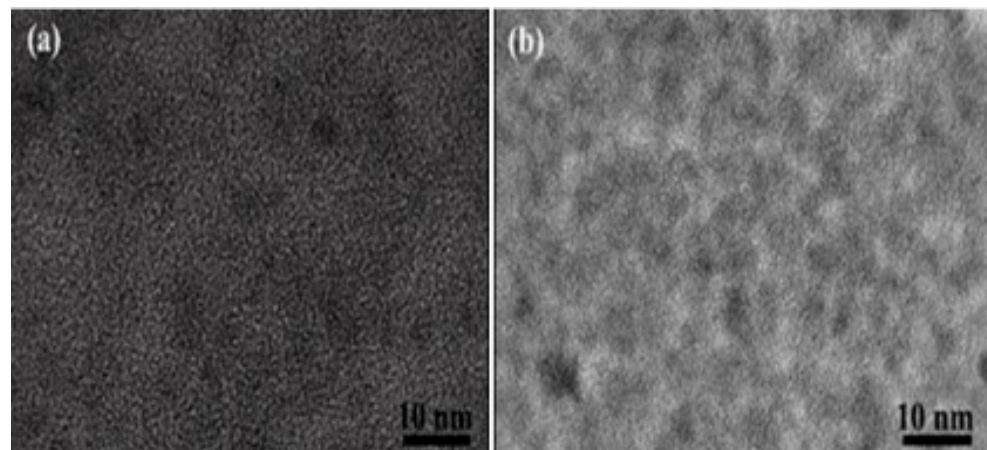


**Figure 6.** (a) HRTEM image of ZCGQDs; (b) HRTEM image of ZCGQDs after  $\text{Cu}^{2+}$  was added.

The addition of metal ions can lead to fluorescence quenching of quantum dots. There are two mechanisms for this phenomenon. One is dynamic quenching, that is, after the quenching agent is added, it can carry out frequent energy transfer between the fluorescent material and reduce the fluorescence lifetime of the material. The other is static quenching, in which the two are mixed together to form a corresponding non-fluorescent complex that shows exactly the specific absorption peak when exposed to UV light.

As shown in Figure 7, after the different concentrations of  $\text{Cu}^{2+}$  were added to the ZCGQDs solutions, their ultraviolet absorption spectra were plotted, and no obvious difference was observed. This indicates that the sol system formed a new non-fluorescent

complex, and the reason for the fluorescence quenching of ZCGQDs complexes by  $\text{Cu}^{2+}$  was the dynamic quenching caused by energy transfer.

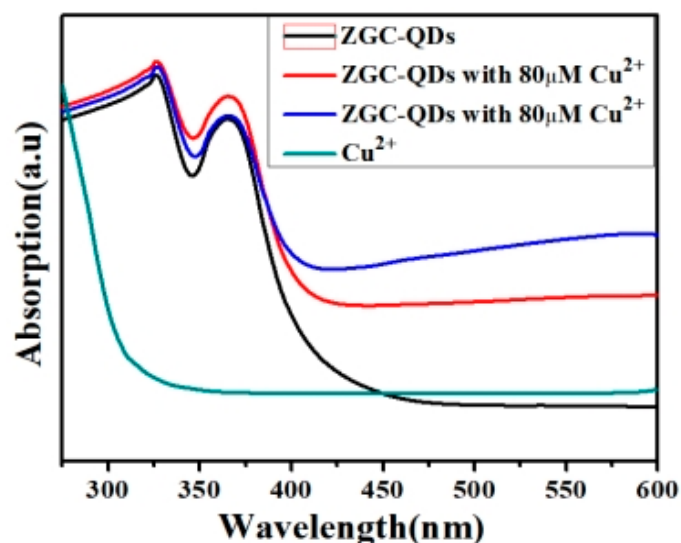


Figure 7. UV-vis absorption spectra of mixed colloids.

#### 4. Conclusions

In this paper, the fluorescence performance of ZCGQDs was analyzed, and it was found that the addition of metal ions would cause the fluorescence intensity of ZCGQDs complexes to weaken, resulting in fluorescence quenching. The fluorescence quenching phenomenon produced by  $\text{Cu}^{2+}$  was the most obvious. Using this principle, the ZCGQDs complexes were used as fluorescent probes to detect  $\text{Cu}^{2+}$ . The mixing time of 15 min makes the most obvious fluorescence burst of  $\text{Cu}^{2+}$  on ZCGQDs with good anti-interference performance. There was a linear relationship between ZCGQDs and  $\text{Cu}^{2+}$  in the range of 1–100  $\mu\text{M}$ , with  $F_0/F = 0.9687 + 0.12343C$ , so the detection limit of  $\text{Cu}^{2+}$  was obtained, which was about 1.74  $\mu\text{M}$ . In addition, the characterization of the materials using transmission electron microscopy and UV spectroscopy proved that  $\text{Cu}^{2+}$  induced the fluorescence quenching of ZCGQDs complexes, which involved the induced aggregation quenching and dynamic quenching.

**Author Contributions:** T.L., L.W. and Y.L.: writing—original draft preparation, writing—review and editing, methodology, formal analysis; R.J., Y.T. and Y.H.: writing—original draft preparation, formal analysis, visualization, project administration; C.S. and S.L.: data analysis; Y.L.: resources. All authors have read and agreed to the published version of the manuscript.

**Funding:** This research was funded by [the Department of Scientific Research Project in Heilongjiang Province] grant number [LH2022B022], and the APC was funded by [Tianze Liu]. [Jiamusi University Horizontal Research Project] grant number [210428001; 021040301], and the APC was funded by [Shuang Liu]. [the Innovation and Entrepreneurship Project for College Students in Heilongjiang Province] grant number [S202210222018], and the APC was funded by [Tianze Liu].

**Data Availability Statement:** The data is unavailable due to privacy or ethical restrictions.

**Conflicts of Interest:** The authors declare no conflict of interest.

#### References

1. Wei, J.R.; Chen, H.Y.; Zhang, W.; Pan, J.X.L.; Dang, F.Q.; Zhang, Z.Q.; Zhang, J. Ratiometric fluorescence for sensitive and selective detection of mitoxantrone using a MIP@rQDs@SiO<sub>2</sub> fluorescence probe. *Sens. Actuators B Chem.* **2017**, *244*, 31–37. [[CrossRef](#)]
2. Qian, J.; Wang, K.; Wang, C.; Ren, C.; Liu, Q.; Hao, N.; Wang, K. Ratiometric fluorescence nanosensor for selective and visual detection of cadmium ions using quencher displacement-induced fluorescence recovery of CdTe quantum dots-based hybrid probe. *Sens. Actuators B Chem.* **2017**, *241*, 1153–1160. [[CrossRef](#)]

3. Gui, W.; Wang, H.; Liu, Y.; Ma, Q. Ratiometric fluorescent sensor with molecularly imprinted mesoporous microspheres for malachite green detection. *Sens. Actuators B Chem.* **2018**, *266*, 685–691. [[CrossRef](#)]
4. Yadav, A.; Upadhyay, Y.; Bera, R.K.; Sahoo, S.K. Vitamin B6 cofactors guided highly selective fluorescent turn-on sensing of histamine using beta-cyclodextrin stabilized ZnO quantum dots. *Food Chem.* **2020**, *320*, 126611. [[CrossRef](#)]
5. Wu, W.J.; Zhao, Q.; Zhou, R.; Linag, Y.C.; Zhao, W.B.; Shan, C.X. Ratiometric fluorescence sensor based on europium-grafted ZnO quantum dots for visual and colorimetric detection of tetracycline. *Spectrochim. Acta Part A Mol. Biomol. Spectrosc.* **2021**, *259*, 119901. [[CrossRef](#)]
6. Omata, T.; Tani, Y.; Kobayashi, S.; Takahashi, K.; Miyanaga, A.; Maeda, Y.; Otsuka-Yao-Matsuo, S. Ultraviolet electroluminescence from colloidal ZnO quantum dots in an all-inorganic multilayer light-emitting device. *Appl. Phys. Lett.* **2012**, *100*, 061104. [[CrossRef](#)]
7. Moyon, E.; Kim, J.H.; Kim, J.; Jinag, J. ZnO nanoparticles for quantum-dot-based light-emitting diodes. *ACS Appl. Nano Mater.* **2020**, *3*, 5203–5211. [[CrossRef](#)]
8. Wang, J.; Lee, J.S.; Kim, D.; Zhu, L. Exploration of zinc oxide nanoparticles as a multitarget and multifunctional anticancer nanomedicine. *ACS Appl. Mater. Interfaces* **2017**, *9*, 39971–39984. [[CrossRef](#)]
9. Tu, Z.; Yang, G.; Song, H.; Wang, C. Amorphous ZnO quantum dot/mesoporous carbon bubble composites for a high-performance lithium-ion battery anode. *ACS Appl. Mater. Interfaces* **2017**, *9*, 439–446. [[CrossRef](#)]
10. Fernando, J.F.S.; Zhang, C.; Firestein, K.L.; Nerkar, J.Y.; Golberg, D.V. ZnO quantum dots anchored in multilayered and flexible amorphous carbon sheets for high performance and stable lithium ion batteries. *J. Mater. Chem. A* **2019**, *7*, 8460–8471. [[CrossRef](#)]
11. Tan, Q.; Kong, X.; Guan, X.; Wang, C.; Xu, B. Crystallization of zinc oxide quantum dots on graphene sheets as an anode material for lithium ion batteries. *Crystengcomm* **2020**, *22*, 320–329. [[CrossRef](#)]
12. Ma, X.; Li, Z.; Chen, D.; Li, Z.; Yan, L.; Li, S.; Liang, C.; Ling, M.; Peng, X. Nitrogen-doped porous carbon sponge-confined ZnO quantum dots for metal collector-free lithium ion battery. *J. Electroanal. Chem.* **2019**, *848*, 113275. [[CrossRef](#)]
13. Jia, Z.; Misra, R.D.K. Tunable ZnO quantum dots for bioimaging: Synthesis and photoluminescence. *Mater. Technol.* **2013**, *28*, 221–227. [[CrossRef](#)]
14. Wu, T.; Wang, Z.; Tian, M.; Miao, H.; Zhang, H.; Sun, J. UVexcitation NO<sub>2</sub> gas sensor sensitized by ZnO quantum dots at room temperature. *Sens. Actuators B Chem.* **2018**, *259*, 526–531. [[CrossRef](#)]
15. Zhao, D.; Song, H.; Hao, L.; Liu, X.; Zhang, L.; Lv, Y. Luminescent ZnO quantum dots for sensitive and selective detection of dopamine. *Talanta* **2013**, *107*, 133–139. [[CrossRef](#)]
16. Jiříčková, A.; Jankovský, O.; Sofer, Z.; Sedmidubský, D. Synthesis and Applications of Graphene Oxide. *Materials* **2022**, *15*, 920. [[CrossRef](#)] [[PubMed](#)]
17. Tiwari, S.; Purabgola, A.; Kandasubramanian, B. Functionalised graphene as flexible electrodes for polymer photovoltaics. *J. Alloy. Compd.* **2020**, *825*, 153954. [[CrossRef](#)]
18. Jafari, E.A.; Moradi, M.; Hajati, S.; Kiani, M.A.; Espinos, J.P. Electrophoretic deposition of mixed copper oxide/GO as cathode and N-doped GO as anode for electrochemical energy storage. *Electrochim. Acta* **2018**, *268*, 392–402. [[CrossRef](#)]
19. Sangeetha, M.; Madhan, D. Ultra sensitive molybdenum disulfide (MoS<sub>2</sub>)/graphene based hybrid sensor for the detection of NO<sub>2</sub> and formaldehyde gases by fiber optic clad modified method. *Opt. Laser Technol.* **2020**, *127*, 106193. [[CrossRef](#)]
20. Zeng, S.; Pan, Q.; Huang, Z.; Gu, C.; Wang, T.; Xu, J.; Yan, Z.; Zhao, F.; Li, P.; Tu, Y.; et al. Ultrafast response of self-powered humidity sensor of flexible graphene oxide film. *Mater. Des.* **2023**, *226*, 111683. [[CrossRef](#)]
21. Zheng, J.; Li, J.; Zhang, L.; Chen, X.; Yu, Y.; Huang, H. Post-graphene 2D materials-based antimicrobial agents: Focus on fabrication strategies and biosafety assessments. *J. Mater. Sci.* **2020**, *55*, 7226–7246. [[CrossRef](#)]
22. Govindaraju, S.; Samal, M.; Yun, K. Superior antibacterial activity of GlcN-AuNP-GO by ultraviolet irradiation. *Mater. Sci. Eng. C* **2016**, *69*, 366–372. [[CrossRef](#)]
23. Gong, J.Q.; He, C.; Zhang, J.L.; Wang, L.Z. GO-P25@SA gel beads with excellent separation performance for photocatalytic degradation of rhodamine B. *Res. Chem. Intermed.* **2021**, *47*, 2331–2338. [[CrossRef](#)]
24. Zhou, C.; He, X.H.; Hou, Y.H.; Zhang, L.; Shi, F.W.; Hu, J.L. Alginate/r-GO/SiO<sub>2</sub> aerogels with double catalytic activity sites and high mechanical performance. *Mater. Lett.* **2021**, *288*, 129394. [[CrossRef](#)]
25. Hosseini, M.G.; Shahryari, E.; Sefidi, P.Y. Polyaniline grafted chitosan/GO-CNT/Fe<sub>3</sub>O<sub>4</sub> nanocomposite as a superior electrode material for supercapacitor application. *J. Appl. Polymer Sci.* **2021**, *138*, e50976. [[CrossRef](#)]
26. Shen, L.; Zhao, W.J.; Wang, K.; Xu, J.G. GO-Ti<sub>3</sub>C<sub>2</sub> two-dimensional heterojunction nanomaterial for anticorrosion enhancement of epoxy zinc-rich coatings. *J. Hazard. Mater.* **2021**, *417*, 126048. [[CrossRef](#)]
27. Huo, X.; Yi, H.; Fu, Y.; An, Z.; Qin, L.; Liu, X.; Li, B.; Liu, S.; Li, L.; Zhang, M.; et al. Porous graphitic carbon nitride nanomaterials for water treatment. *Environ. Sci. Nano* **2021**, *8*, 1835–1862. [[CrossRef](#)]
28. Shi, H.; Long, S.; Hou, J.; Ye, L.; Sun, Y.; Ni, W.; Song, C.; Li, K.; Gurzadyan, G.G.; Guo, X. Defects promote ultrafast charge separation in graphitic carbon nitride for enhanced visible-light-driven CO<sub>2</sub> reduction activity. *Chem. Eur. J.* **2019**, *25*, 5028–5035. [[CrossRef](#)]
29. Akple, M.S.; Ishigaki, T.; Madhusudan, P. Bio-inspired honeycomb-like graphitic carbon nitride for enhanced visible light photocatalytic CO<sub>2</sub> reduction activity. *Environ. Sci. Pollut. Res.* **2020**, *27*, 22604–22618. [[CrossRef](#)] [[PubMed](#)]
30. Sharma, R.; Almáši, M.; Nehra, S.P.; Rao, V.S.; Panchal, P.; Paul, D.R.; Jain, I.P.; Sharma, A. Photocatalytic hydrogen production using graphitic carbon nitride (GCN): A precise review. *Renew. Sustain. Energy Rev.* **2022**, *168*, 112776. [[CrossRef](#)]

31. Li, L.; Yu, H.; Xu, J.; Zhao, S.; Liu, Z.; Li, Y. Rare earth element, Sm, modified graphite phase carbon nitride heterostructure for photocatalytic hydrogen production. *New J. Chem.* **2019**, *43*, 1716–1724. [[CrossRef](#)]
32. Wang, Y.; Liu, L.; Ma, T.; Zhang, Y.; Huang, H. 2D graphitic carbon nitride for energy conversion and storage. *Adv. Funct. Mater.* **2021**, *31*, 2102540. [[CrossRef](#)]
33. Niu, W.; Yang, Y. Graphitic carbon nitride for electrochemical energy conversion and storage. *ACS Energy Lett.* **2018**, *3*, 2796–2815. [[CrossRef](#)]
34. Yang, Y.; Zou, T.; Zhao, R.; Kong, Y.; Su, L.; Ma, D.; Xiao, X.; Wang, Y. Fluorescence ‘turn-on’ probe for Al<sup>3+</sup> detection in water based on ZnS/ZnO quantum dots with excellent selectivity and stability. *Nanotechnology* **2021**, *31*, 2102540. [[CrossRef](#)]
35. Zhan, M.; Jia, H.; Fan, J.; Yu, H.; Amador, E.; Chen, W. Two D-pi-A schiff-base-functionalized silica gel adsorbents for preconcentration of copper ions in foods and water for detection. *Anal. Chem.* **2019**, *91*, 6103–6110. [[CrossRef](#)] [[PubMed](#)]
36. Karakus, E. A rhodamine based fluorescent chemodosimeter for the selective and sensitive detection of copper(II) ions in aqueous media and living cells. *J. Mol. Struct.* **2021**, 1224. [[CrossRef](#)]
37. Falina, S.; Syamsul, M.; Rhaffor, N.A.; Hamid, S.S.; Zain, K.A.M.; Manaf, A.A.; Kawarada, H. Ten years progress of electrical detection of heavy metal ions(HMIs) using various field-effect transistor (FET) nanosensors: A review. *Biosensors* **2021**, *11*, 478. [[CrossRef](#)]
38. Guo, W.; Zhang, C.; Ma, T.; Liu, X.; Chen, Z.; Li, S.; Deng, Y. Advances in aptamer screening and aptasensors’ detection of heavy metal ions. *J. Nanobiotechnol.* **2021**, *19*, 166. [[CrossRef](#)]
39. Chen, S.-H.; Li, Y.-X.; Li, P.-H.; Xiao, X.-Y.; Jiang, M.; Li, S.-S.; Zhou, W.-Y.; Yang, M.; Huang, X.-J.; Liu, W.-Q. Electrochemical spectral methods for trace detection of heavy metals: A review. *TrAC Trends Anal. Chem.* **2018**, *106*, 139–150. [[CrossRef](#)]
40. Zhu, X.; Chen, L.; Lin, Z.; Qiu, B.; Chen, G. A highly sensitive and selective “signal-on” electrochemiluminescent biosensor for mercury. *Chem. Commun.* **2010**, *46*, 3149–3151. [[CrossRef](#)] [[PubMed](#)]
41. Zhu, Y.; Jiang, X.; Wang, H.; Wang, S.; Wang, H.; Sun, B.; Su, Y.; He, Y. A poly adenine-mediated assembly strategy for designing surface-enhanced resonance raman scattering substrates in controllable manners. *Anal. Chem.* **2015**, *87*, 6631–6638. [[CrossRef](#)]
42. Roy, A.; Nlandi, M.; Roy, P. Dual chemosensors for metal ions: A comprehensive review. *TrAC Trends Anal. Chem.* **2021**, *138*, 116204. [[CrossRef](#)]
43. Peng, J.; Li, J.; Xu, W.; Wang, L.; Su, D.; Teoh, C.L.; Chang, Y.-T. Silica nanoparticle-enhanced fluorescent sensor array for heavy metal ions detection in colloid solution. *Anal. Chem.* **2018**, *90*, 1628–1634. [[CrossRef](#)]
44. Yang, X.; Li, Z.; Liu, N.; Song, W.; Sun, Q.; Xie, Y. Fabrication of hydrophilic luminescent zinc oxide quantum dots for selective detection of copper ions and efficient inhibition of harmful fungi. *Arab. J. Chem.* **2022**, *15*, 104266. [[CrossRef](#)]
45. Ng, S.M.; Chin, S.F. Interface study on zinc oxide quantum dots using fluorometric and regression analysis in view of optical sensing. *Anal. Lett.* **2013**, *46*, 1278–1288. [[CrossRef](#)]
46. Moussa, H.; Merlin, C.; Dezanet, C.; Balan, L.; Medjahdi, G.; Ben-Attia, M.; Schneider, R. Trace amounts of Cu<sup>2+</sup> ions influence ROS production and cytotoxicity of ZnO quantum dots. *J. Hazard. Mater.* **2016**, *304*, 532–542. [[CrossRef](#)]
47. Zou, T.; Xing, X.; Yang, Y.; Wang, Z.; Wang, Z.; Zhao, R.; Zhang, X.; Wang, Y. Water-soluble ZnO quantum dots modified by (3-aminopropyl) triethoxysilane: The promising fluorescent probe for the selective detection of Cu<sup>2+</sup> ion in drinking water. *J. Alloys Compd.* **2020**, *825*, 153904. [[CrossRef](#)]
48. Khan, M.M.R.; Mitra, T.; Sahoo, D. Metal oxide QD based ultrasensitive microsphere fluorescent sensor for copper, chromium and iron ions in water. *RSC Adv.* **2020**, *10*, 9512–9524. [[CrossRef](#)]
49. Ng, S.M.; Wong, D.S.N.; Phung, J.H.C.; Chua, H.S. Integrated miniature fluorescent probe to leverage the sensing potential of ZnO quantum dots for the detection of copper (II) ions. *Talanta* **2013**, *116*, 514–519. [[CrossRef](#)]

**Disclaimer/Publisher’s Note:** The statements, opinions and data contained in all publications are solely those of the individual author(s) and contributor(s) and not of MDPI and/or the editor(s). MDPI and/or the editor(s) disclaim responsibility for any injury to people or property resulting from any ideas, methods, instructions or products referred to in the content.